Journal of Nanobiotechnology

RESEARCH

Open Access

NIR-activatable nitric oxide generator based on nanoparticles loaded small-molecule photosensitizers for synergetic photodynamic/gas therapy

Lili Fu[1,3], Yan Huang[1*], Xin Shan[4], Xiao Sun[1], Xinlei Wang[1], Xiaoyan Wang[1], Lingxin Chen[1,2*] and Shui Yu[1*]

Abstract

Background Therapeutic approaches that combine conventional photodynamic therapy (PDT) with gas therapy (GT) to sensitize PDT are an attractive strategy, but the molecular structure design of the complex lacks effective guiding strategies.

Results Herein, we have developed a nanoplatforms Cy-NMNO@SiO_2 based on mesoporous silica materials loaded NIR-activatable small-molecule fluorescent probe Cy-NMNO for the synergistic treatment of photodynamic therapy/gas therapy (PDT/GT) in antibacterial and skin cancer. The theoretical calculation results showed that the low dissociation of N-NO in Cy-NMNO enabled it to dissociate effectively under NIR light irradiation, which is conducive to produce Cy and NO. Cy showed better $^1O_2$ generation performance than Cy-NMNO. The cytotoxicity of Cy-NMNO obtained via the synergistic effect of GT and PDT synergistically enhances the effect of photodynamic therapy, thus achieving more effective tumor treatment and sterilization than conventional PDT. Moreover, the nanoplatforms Cy-NMNO@SiO_2 realized efficient drug loading and drug delivery.

Conclusions This work not only offers a promising approach for PDT-GT synergistic drug delivery system, but also provides a valuable reference for the design of its drug molecules.

Keywords Photodynamic therapy, Nanoplatforms, Mesoporous silica materials, Small-molecule photosensitizers, Nitric oxide release

*Correspondence:
Yan Huang
yhuang@yic.ac.cn
Lingxin Chen
lxchen@yic.ac.cn
Shui Yu
yushui_0121@163.com

Full list of author information is available at the end of the article

Graphical Abstract

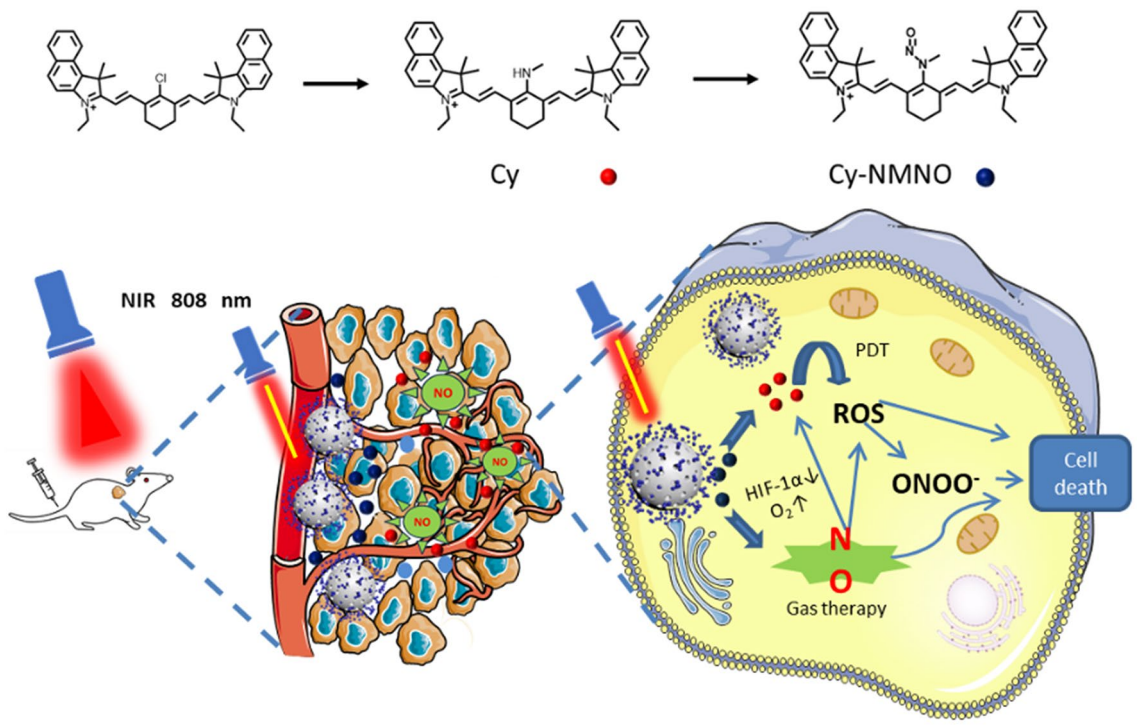

Introduction

In recent years, photodynamic therapy (PDT), an antimicrobial and antitumor treatment modality that kills tumor cells and bacteria by converting oxygen (O_2) into cytotoxic reactive oxygen species (ROS) through irradiation of photosensitizers with minimal invasiveness to normal tissues, has received a lot of attention from researchers [1–6]. Despite the numerous advantages and recent advances in PDT, its clinical translation is limited due to pre-existing hypoxia within tumor tissues. Gas therapy (GT) based on nitric oxide (NO) is considered a new "green" therapy that can effectively overcome hypoxia gradients, and its release is independent of the O_2 availability [7]. NO-mediated vasodilation increases blood perfusion, which then effectively relieves hypoxia at the tumor, with negligible side effects [8]. High concentrations of NO (>1 μM) not only significantly inhibit tumorigenesis, but also synergistically improve the efficacy of chemotherapy, photodynamic therapy, photothermal therapy, or radiation therapy. In addition, NO can react with ROS to produce more toxic reactive nitrogen species (RNS), such as peroxynitrite ($ONOO^-$), and these molecules exacerbate DNA breakage and trigger apoptosis, ultimately enhancing the therapeutic effect of ROS on cancer cells and bacteria [9–11]. Therefore, combining NO with PDT therapy may be a promising strategy for hypoxic tumor treatment and antimicrobial. Based on this strategy, researchers have designed and reported some complexes that can simultaneously produce ROS and NO, showing significant tumor treatment effects [12]. Noteworthy, the performance of complexes is influenced by two factors. Firstly, the dissociation ability of NO from the complex under illumination affects the NO content, which in turn affects the performance of GT. Secondly, the ROS generation ability of the matrix molecules after NO release will further affect the PDT performance. Therefore, the structural design of complex should fully consider the above factors, yet most of the current studies lack theoretical support in this regard.

Near-infrared (NIR) laser-triggered photodynamic therapy based on various nano-agents is one of the most effective anti-tumor strategies due to its high spatial resolution and depth of tissue penetration. In addition, NIR lasers can be focused on the target area to promote blood circulation and relieve tissue inflammation. In particular, NIR light exhibits low phototoxicity compared to shorter wavelengths such as UV or blue light. While anthocyanine dyes not only have excellent optical properties, including high molar extinction coefficient, high fluorescence quantum yield, adjustable absorption and emission wavelength range (from visible to near-infrared region), but also have the advantages of low cytotoxicity, good biocompatibility and low autofluorescence background interference [13, 14]. In addition, the anthocyanine dye

can also act as a photosensitizer under near-infrared light irradiation, producing excellent PDT therapeutic effects on tumor cells and bacteria [15]. It has been reported in the literature that the -NNO structure with strong electron absorbing capacity is a typical functional group for the release of nitric oxide (NO) from tumor GT under irradiation, which is converted to -NH with good electron supplying capacity. Therefore, using anthocyanins as photosensitizers and NO delivery agents is expected to achieve the GT and PDT synergistic enhancement of anti-tumor performance under NIR conditions. In addition, with the rapid development of bio-nanotechnology, nanomaterials have also shown good application prospects in drug delivery systems (DDSs) due to their special properties [16]. Among the many nanomaterials as DDSs, mesoporous silica nanoparticles (MSNs), as a type of nanomaterials, have become a hot research topic in DDSs due to their unique mesoporous structure, large pore volume, high specific surface area, good biocompatibility, and easy modification of the surface hotspot of research [17, 18]. The current study shows that MSN is less toxic than other nanocarriers, including carbon nanotubes [19]. The enhanced permeability and retention (EPR) effects suggest that MSN may be an excellent candidate for cancer therapy [20]. The ability of MSN to target cells, be taken up and retained in the circulation is a clinical manifestation of the selectivity and toxicity of DDS [21].

In previous studies, nanoplatforms were often combined with multiple therapeutic modalities such as PDT, photothermal therapy (PTT), and GT, without addressing the diagnostic function [22]. Here, we designed an integrated diagnostic and therapeutic fluorescent probe, Cy-NMNO, which rationalized the development of an NIR-activatable and multifunctional platform for synergistic GT and PDT by linking the NIR fluorescent dye cyanidin to nitrosamine. It was then loaded into mesoporous silica to form a nanoplatform for drug loading and drug delivery (Scheme 1). Notably, the low dissociation of N-NO in Cy-NMNO enabled it to dissociate effectively, which is conducive to the release of NO. In addition, Cy obtained by releasing NO showed better $^1O_2$ generation performance than Cy-NMNO. The cytotoxicity of Cy-NMNO obtained through the synergistic effect of GT and PDT is an excellent probe that effectively alleviates hypoxia at the tumor site and significantly improves the hypoxic environment caused by PDT in an all-in-one treatment, achieving effective antitumor therapy at the skin cancer site through PDT/GT. Due to the continuous development of photodynamics, antimicrobial agents based on photodynamic therapy are also being used more and more widely. Therefore, we applied the nanoplatform Cy-NMNO@SiO_2 to antimicrobial therapy as well. We found that the nanoplatform Cy-NMNO@SiO_2 was equally capable of producing a synergistic PDT/GT effect on both Gram-positive and Gram-negative bacteria, realizing a broad-spectrum antimicrobial effect. We designed nanoplatform Cy-NMNO@SiO_2 has the potential to be an antimicrobial antitumor therapeutic strategy and provide a research basis for clinical antimicrobial antitumor drug studies.

Experimental methods

The list of instruments, materials, synthetic methods, results of the chemical analysis and flow cytometry are listed in the ESI.†

Synthesis of Cy

Under the protection of argon, phlorocyanine dye with benzindole heterocyclic ring (0.611 g, 1 mmol) and methylamine hydrochloride (0.675 g, 10 mmol) were dissolved in 10 mL of N, N-dimethylformamide (DMF), and then triethylamine (1.012 g, 10 mmol) was added dropwise to the mixture dissolved by DMF, and stirred under the condition of 40 ℃ until the color of the solution was changed from green to blue. After the reaction, the product was extracted with CH_2Cl_2, washed with ultrapure water for 5 times, and dried under vacuum to obtain the blue product. The crude product was purified by silica gel chromatography and eluted with EtOAc/CH_3OH (5:1, v/v) to obtain the blue solid compound Cy. ^{1}H NMR ($CDCl_3$-d_1, 500 MHz) δ (ppm): 10.36 (s, 1H), 8.13–8.12 (d, 2 H), 7.86–7.82 (m, 6 H), 7.54–7.52 (m, 2 H), 7.35 (s, 2 H), 7.17–7.15 (m, 2 H), 5.59–5.56 (d, 2 H), 3.95–3.93 (m, 4 H), 3.78–3.60 (m, 4 H), 2.58–2.56 (m, 4 H), 2.02–1.85 (m, 11 H), 1.67 (m, 2 H), 1.40–1.27 (m, 6 H). ^{13}C NMR ($CDCl_3$-d_1, 125 MHz) δ (ppm): 170.29, 167.37, 154.49, 140.01, 135.96, 131.49, 130.56, 129.74, 129.71, 129.63, 128.75, 127.24, 123.45, 122.15, 119.04, 109.64, 109.19, 92.20, 49.28, 37.67, 37.25, 28.12, 26.18, 21.25, 11.61. LC-MS (ESI$^+$): m/z $C_{43}H_{48}N_3^+$ calcd. 606.3843, found [M^+] 606.5778.

Synthesis of Cy-NMNO

The blue solid compound Cy (0.606 g, 1 mmol), $NaNO_2$ (0.069 g, 1 mmol) was dissolved in 10 mL of methanol under an ice bath, stirred for 20 min and then acetic acid (0.060 g, 1 mmol) was added to the reaction for 3 h. At the end of the reaction, the product was extracted with CH_2Cl_2, washed with ultrapure water for 5 times, and dried in vacuum to obtain the blue product. The crude product was purified by silica gel chromatography and eluted with CH_2Cl_2/CH_3OH (8:1, v/v) to obtain the probe Cy-NMNO. ^{1}H NMR (MeOD-d_4, 500 MHz) δ (ppm): 8.17–8.16 (d, 2 H), 7.93–7.91 (m, 4 H), 7.86–7.83 (d, 2 H), 7.57–7.54 (m, 2 H), 7.43–7.41 (d, 2 H), 7.39–7.37 (m, 2 H), 5.83–5.80 (d, 2 H), 4.11–4.10 (m, 4 H), 3.33–3.32 (t, 4 H), 2.63–2.61 (m, 3 H), 1.97 (s, 12 H), 1.39–1.29 (m,

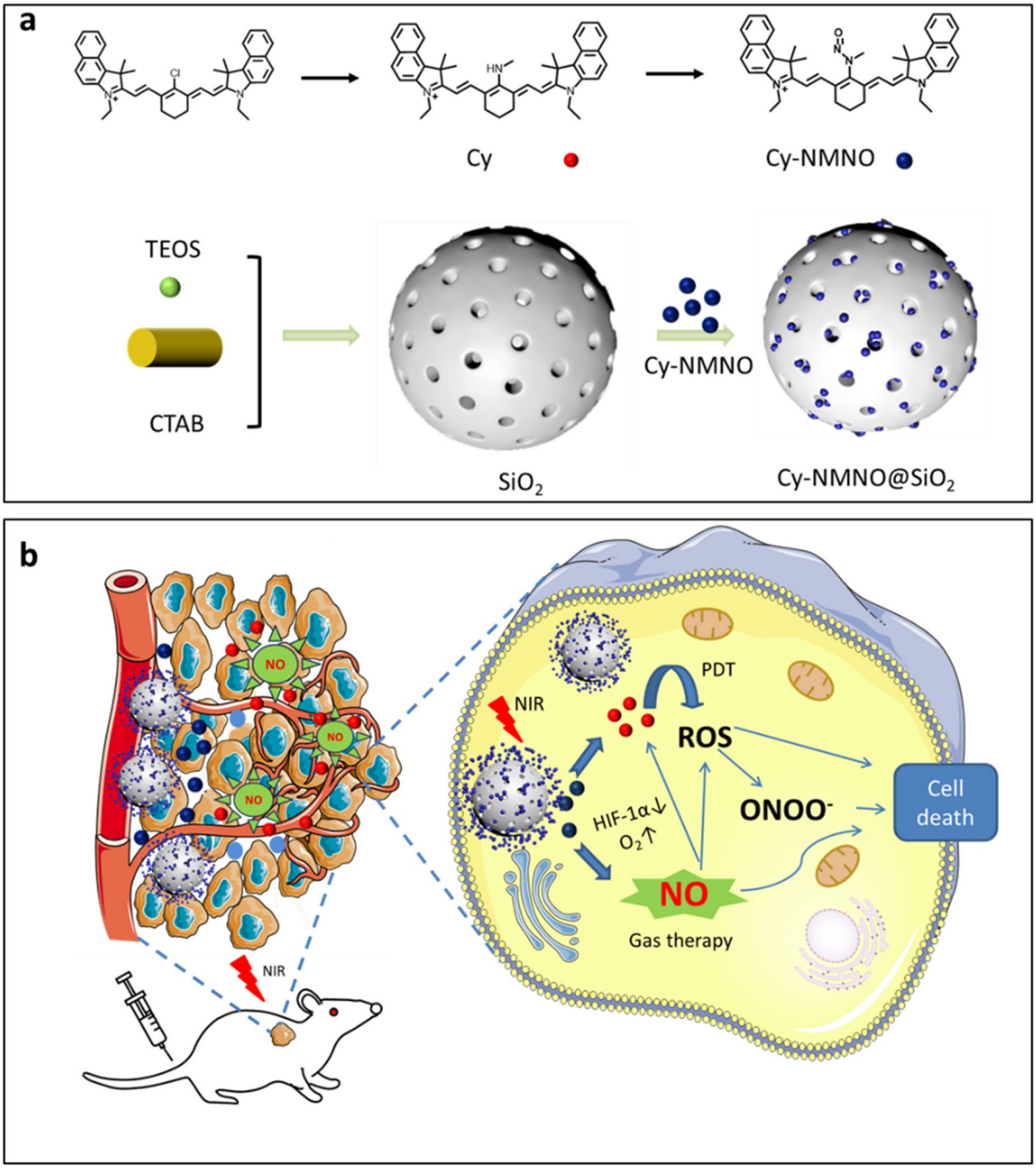

Scheme 1 (**a**) Schematic illustration of the synthesis route of Cy-NMNO@SiO_2. (**b**) The mechanism of the Cy-NMNO@SiO_2 for the PDT/GT

8 H). ^{13}C NMR (MeOD-d_4, 125 MHz) δ (ppm): 168.2, 142.3, 139.7, 138.0, 136.8, 136.7, 131.7, 130.9, 129.8, 129.6, 128.5, 126.8, 123.2, 121.5, 115.9, 109.6, 107.5, 97.1, 92.8, 62.6, 54.9, 36.3, 29.3, 27.0, 25.5, 22.3, 21.2, 13.0, 10.6. LC-MS (ESI^+): m/z $C_{43}H_{47}N_4O^+$ calcd.635.37, found [M^+] 635.29.

Synthesis of SiO2

SiO_2 were synthesized based on available literature [23]. Hexadecyl trimethyl ammonium Bromide (CTAB, 200 mg) was dissolved in distilled water (100 mL) and then NaOH aqueous solution (0.7 mL, 2 M) was added. The mixture was stirred at 80 °C for 30 min and then Tetraethyl orthosilicate (TEOS, 1 mL) was added with vigorous stirring. Stirring was continued for 4 h. The mixture was allowed to cool to room temperature and

the precipitate was collected by filtration. The products (MSNs) were washed three times thoroughly with deionized water and ethanol and dried under vacuum at room temperature for 2 days. The final product was heated in a muffle furnace at 500 °C for 5 h to remove the CTAB.

Synthesis of Cy-NMNO@SiO2

The mesoporous silica was immersed in Cy, Cy-NMNO solution, respectively, and then the suspension was physically stirred to load the small molecule photosensitizer into the mesoporous structure. Vacuum filtration and decompression drying remove the solvent and the nanoparticles can be isolated.

Establishment of A375 tumor xenograft model mice

Establishing A375 tumor xenografts models, Athymic nude mice (aged 4–5 weeks, weighing 18–20 g) were purchased from Binzhou Medical University. For the A375 tumor xenografts, 2×10^6 A375 cancer cells suspended in 200 μL PBS were subcutaneously implanted into the right flank of each athymic nude mouse. All animals were maintained under aseptic conditions and were housed in groups of five in standard cages with free access to food and water and a 12 h light/dark cycle. The tumor is allowed to grow for about 8–10 days until it reaches a volume of 150 mm^3.

Statistical analysis

All results were analyzed using GraphPad Prism 9.5 software, and the results were expressed as the mean ± standard deviation (SD) of three measurements per experiment. The significance of differences between groups was determined with one-way ANOVA and t-test analysis. The significance levels were $^{*}p<0.05$, $^{**}p<0.01$, $^{***}p<0.001$ and $^{****}p<0.0001$.

Ethical statement

All animal procedures were performed in accordance with the Guidelines for Care and Use of Laboratory Animals of Binzhou Medical University and approved by the Institutional Animal Care and Use Committee of Binzhou Medical University (Yantai, China) (Approval Number: 2023−125).

Results and discussion

Design strategy for nanoplatform Cy-NMNO@SiO_2

Scheme 1a outlines the synthesis of nanoplatform Cy-NMNO@SiO_2. All synthesized compounds were confirmed by ^{1}H NMR, ^{13}C NMR and liquid chromatography ion trap mass spectrometry (LC-MS). The synthesis details of the nanoplatforms are shown in the Supporting Information. Typically, hypoxia is one of the major therapeutic barriers to PDT, whereas hyperoxia promotes ROS production and enhances the killing effect on tumors and bacteria. Therefore, we first designed a fluorescent probe, Cy-NMNO, which can release both NO and photosensitizer under near-infrared laser irradiation for the treatment of tumors and antibacterials and to ameliorate the hypoxia problem in photodynamic therapy (Scheme 1b). In this scheme, we chose a benzoheptamethine cyanine dye with a benzo-indole heterocycle as a photosensitizer, which is due to the fact that when the heterocycle in the structure of the benzoheptamethine cyanine dye is changed from an indole heterocycle to a benzo-indole heterocycle, the nature of the push-pull electronic structure of the a benzoheptamethine cyanine dye is changed. This affects the conjugated nature of the phorbol ester system, resulting in a red shift in the absorption and fluorescence spectra, which gives it a longer near-infrared excitation wavelength and improves the shortcomings of the traditional laser light scattering. And it can penetrate deeper tissues and thus excite more photosensitizer-enriched regions. We then combined the nitrosamine group with the fluorophore Cy to obtain the compound Cy-NMNO with a high molar absorption coefficient and near-infrared (NIR) emission.

In addition, MSN particle size controls cellular interactions as well as distribution and elimination. It has been reported in the literature that the optimal MSN size to promote accumulation at the tumor site and provide a longer circulating half-life is in the range of 50–300 nm. Smaller MSNs (less than 50 nm) have poor porosity, while larger MSNs (greater than 300 nm) have impaired diffusion into the tumor mesenchyme [24]. Therefore, we synthesized MSNs with sizes around 50–100 nm for loading small molecule photosensitizers.

Characterization of Cy-NMNO@SiO2

Cy-NMNO@SiO_2 was then characterized in detail. Transmission electron microscopy (TEM) imaging and DLS analysis showed that the size of Cy-NMNO@SiO_2 was about 50–100 nm with good particle homogeneity (Fig. 1a and b). The spectral properties of Cy@SiO_2, Cy-NMNO@SiO_2 were investigated under simulated physiological conditions (10 mM HEPES, pH 7.4). As shown in Fig. 1c, Cy@SiO_2 has a strong absorption around 800 nm, which is favorable for its application in NIR laser-based photodynamic therapy. After substitution and nitration of the exposed amino group, the electron-donating ability of the amino group is greatly reduced, leading to the PET process accompanied by fluorescence burst. We hypothesized that under the excitation of 808 nm light, the uniform breakage of the N-N bond leads to the departure of the substituent and the fluorescence turns on. To verify the role of Cy-NMNO@SiO_2 in response to NIR laser light, we divided the Cy-NMNO@SiO_2 solution into two groups. The fluorescence activation behavior in the NIR was verified by fluorescence spectroscopy.

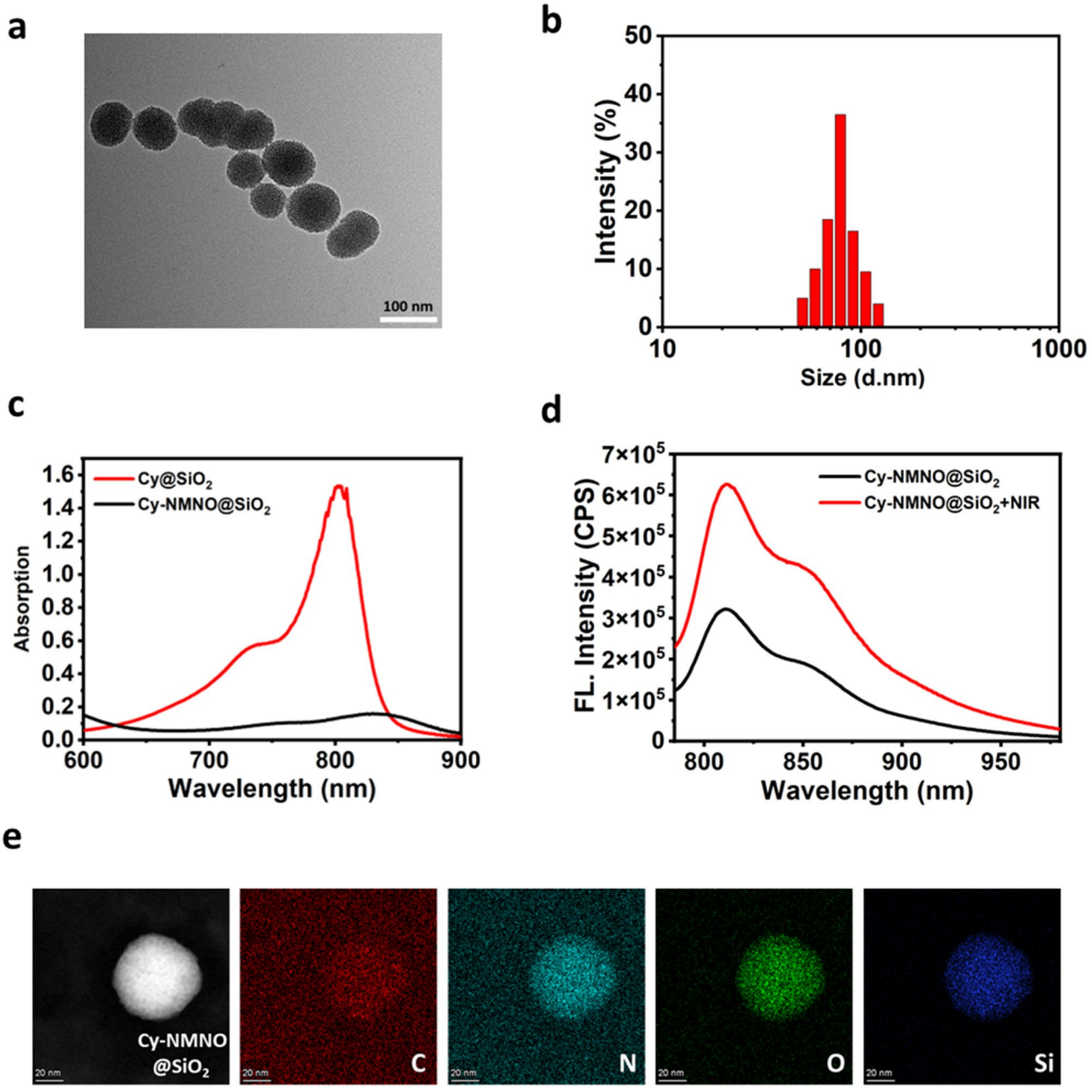

Fig. 1 (**a**) A representative TEM image for Cy-NMNO@SiO_2. (**b**) DLS data of the Cy-NMNO@SiO_2. (**c**) Absorption spectra of Cy@SiO_2, Cy-NMNO@SiO_2. (**d**) After laser irradiation (5 min, 808 nm), the fluorescence emission spectrum of Cy-NMNO@SiO_2 changed. All data were collected in HEPES (pH 7.4) at 37 ℃ (λ_{ex} = 730 nm, λ_{em} = 810 nm). (**e**) EDS elemental mapping of Cy-NMNO@SiO_2. Scale bar = 20 nm

As shown in Fig. 1d, the fluorescence emission intensity of Cy-NMNO@SiO_2 solution after NIR laser irradiation was significantly enhanced, reaching the maximum emission wavelength at 810 nm. Both the maximum absorption wavelength and fluorescence emission wavelength were located in the near-infrared region. Energy dispersive X-ray spectroscopy (EDS) elemental mapping (Fig. 1e) showed that Cy-NMNO is uniformly distributed in mesoporous silica.

Study on the activation and release of Cy-NMNO@SiO_2 in vitro

To demonstrate that our synthesized nanoplatforms have the function of activation under NIR light irradiation, we imaged the live cells with confocal laser scanning microscopy (CLSM) to observe the activation process. Human malignant melanoma cells (A375 cells) were treated with Cy-NMNO@SiO_2 (6 μg/mL) for 2 h, washed, and subjected to NIR laser irradiation (808 nm, 5 min, 1.5 W cm^{-2}). The cells were then washed three

times with Dulbecco's modified eagle medium (DMEM) to remove excess Cy-NMNO@SiO_2. As shown in Fig. 2a, there was almost no fluorescence in the cell group irradiated by NIR laser alone with the addition of Cy-NMNO@SiO_2 alone. In contrast, after incubation and irradiation with the addition of Cy-NMNO@SiO_2, significant fluorescence appeared in the cells, and the fluorescence signal became stronger and stronger. The mean fluorescence intensity was shown in Fig. 2d. These results indicated that the nanoplatform was able to deliver the probe into tumor cells and activate it under NIR laser irradiation. We further validated the obtained results by flow cytometry analysis Fig. 2c.

Inspired by the well-characterized cascade reaction of Cy-NMNO@SiO_2 in solution, in vitro assays were performed to visualize the intracellular NO and $^1O_2$ production in Cy-NMNO@SiO_2 cells by laser confocal microscopy using DAF-FM (a commercial NO probe) and single-linear-state oxygen green sensor (SOSG) fluorescent probes, respectively, to visualize the Cy-NMNO@SiO_2 intracellular $^1O_2$/NO production. As a result, both the NIR group alone and the cells treated with Cy-NMNO@SiO_2 alone showed fluorescence intensities similar to the background signal (Fig. 2b). However, in the Cy-NMNO@SiO_2+NIR group had enhanced fluorescence, which indicated that the probe was effectively released to produce $^1O_2$ with NO under 808 nm near-infrared laser irradiation, and $^1O_2$ was produced by photosensitizer under laser irradiation. In addition, it has been shown in the literature that NO can react with superoxide anions in the tumor environment to form the oxidant peroxynitrite ($ONOO^-$), which stimulates the production of matrix metalloproteinases (MMPs) in the tumor mesenchyme, thereby degrading virtually all of the collagenous components of the ECM and facilitating the penetration of therapeutic agents at the tumor site [25]. Therefore, we used TPNIR-FP detection to show that $ONOO^-$ was indeed produced during the process.

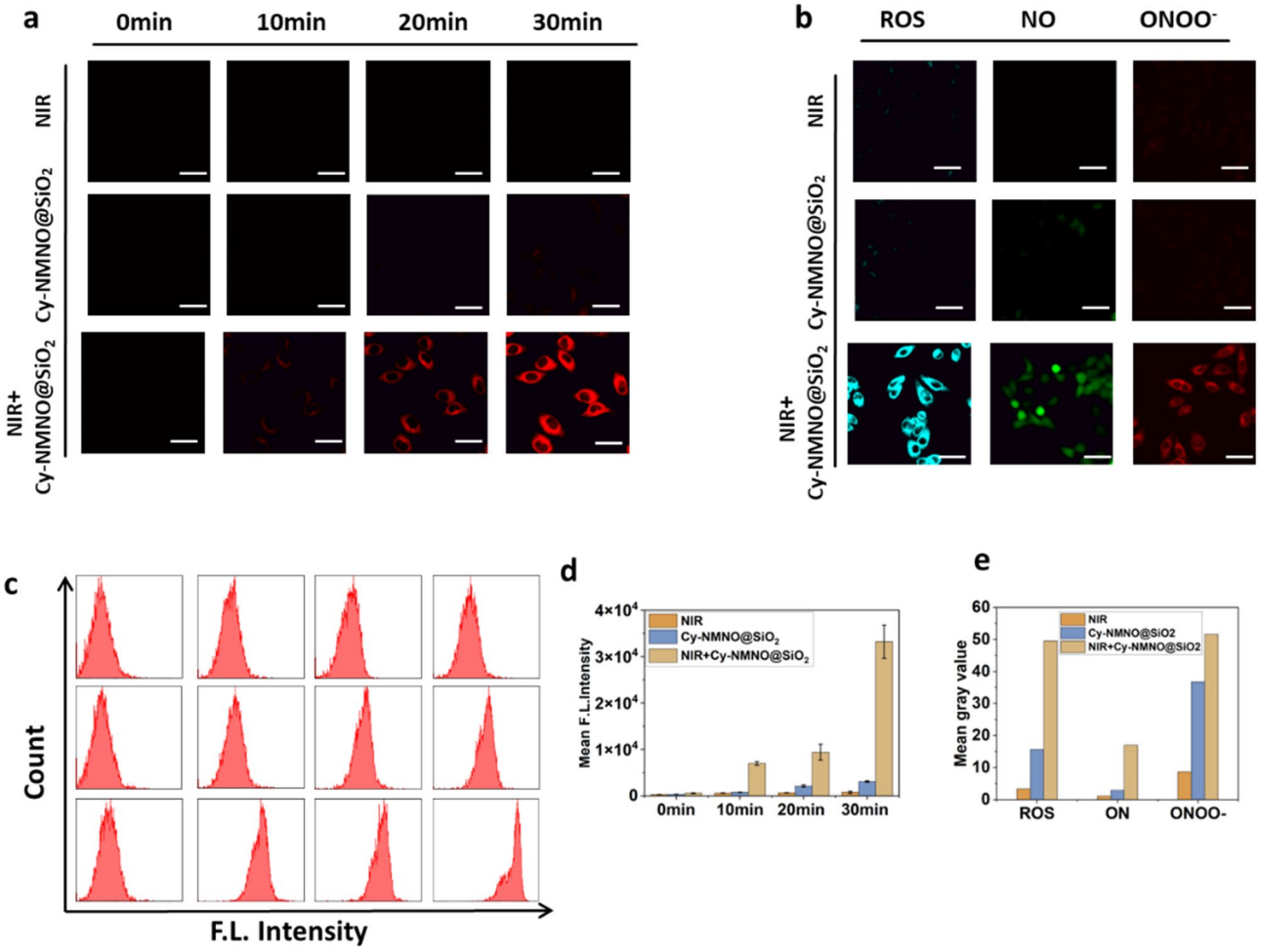

Fig. 2 (**a**) Photographs of fluorescence brightness at different incubation times under laser confocal microscopy for the NIR group, Cy-NMNO@SiO_2 group, and the NIR + Cy-NMNO@SiO_2 group. Scale bar = 20 μm. (**b**) ROS, NO and $ONOO^-$ production in A375 cells were detected by SOSG, DAF-FM, TPNIR-FP probes, respectively. Scale bar = 20 μm. (**c**) The flow cytometry analysis of (**a**). (**d**) The mean gray value of (**a**). (**e**) The mean gray value of (**b**). Mean fluorescence intensity (Mean) = Sum of fluorescence intensities in the area (IntDen) / Area of the region (Area)

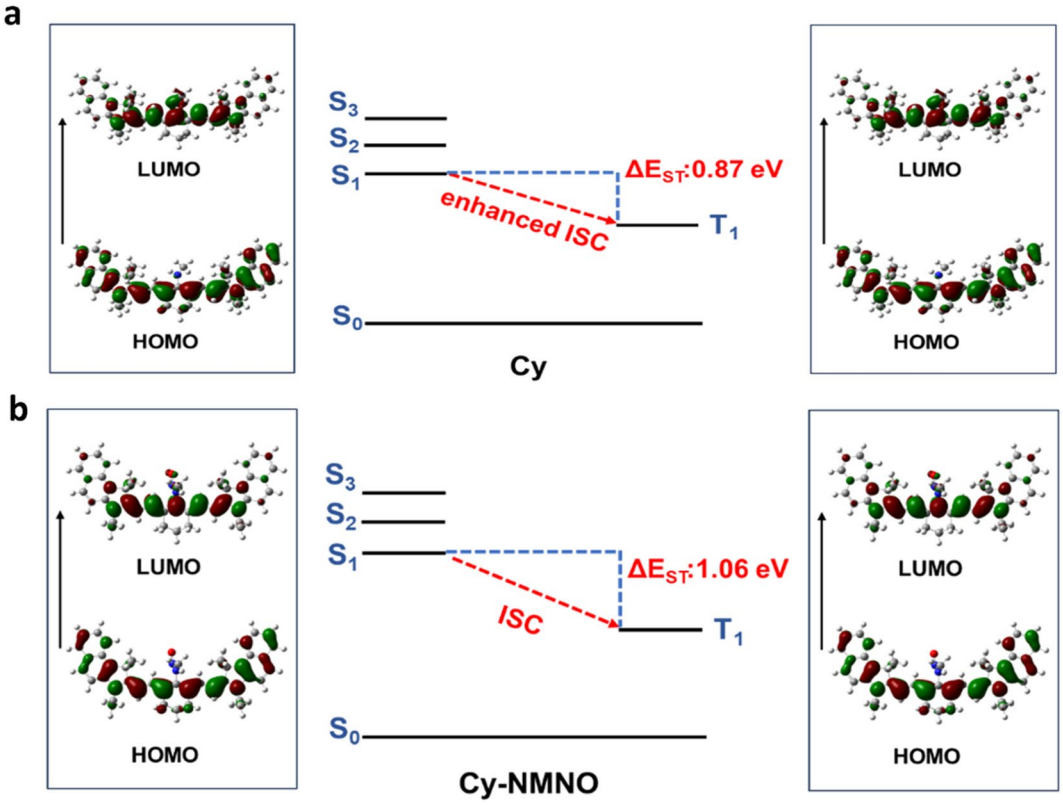

Fig. 3 Selected frontier molecular orbitals involved in excitation and singlet/triplet excited states of Cy (**a**), and Cy-NMNO (**b**)

These results indicate that the photoactivation of Cy-NMNO@SiO_2 in living cells is successful and produces potent class I and class II responses due to the photorelease of ·NO, providing the basis for a synergistic anti-hypoxic photodynamic effect. The above results indicate that the fracture response properties of the probe can specifically respond to NIR light, and that fracture produces both photosensitizer and NO, and in the process, additionally generates $ONOO^-$, which enhances the phototoxicity of Cy. Meanwhile, we quantitatively analyzed the fluorescence intensity in Fig. 2d and 2e using ImageJ software.$^1O_2$, NO and $ONOO^-$ were all significantly enhanced under laser irradiation. Mean fluorescence intensity (Mean) = Sum of fluorescence intensities in the area (IntDen) / Area of the region (Area).

According to the above experimental results, Cy-NMNO showed excellent NO and $^1O_2$ production performance. Theoretical calculations were used to reveal the effect of the molecular structure of Cy-NMNO on the NO and $^1O_2$ production. The ability of NO to dissociate from Cy-NMNO under NIR irradiation determines the NO content. The dissociation ability can be evaluated by the bond dissociation energy (BDE) of N-NO. The bond dissociation energy (BDE) for Cy-NMNO was calculated as 32.8 kcal/mol (Figure S2). The photon energy of 808 nm infrared light is 35.4 kcal/mol, which can realize N-NO bond breaking of Cy-NMNO under NIR irradiation. In addition, we also calculated the N-NO BDE of the molecule reported in the literature. The results showed that the value of BDE is closely related to the molecular structure (Figure S2). Therefore, screening suitable photosensitizers can regulate the NO release performance by affecting BDE of N-NO bond, which provides a reference for the synthesis of complex.

The N-NO bond of the Cy-NMNO breaks under NIR light irradiation, releasing the small molecule photosensitizer Cy. The performance difference between Cy-NMNO and Cy for $^1O_2$ generation will affect the PDT performance. Efficient intersystem crossing (ISC) offers the opportunity to improve the triplet excited state yield, which is highly desirable for efficient $^1O_2$ generation [26]. The small ΔE_{ST} (the energy gap between singlet excited state and triplet excited state) is favor to improve the ISC process. TDDFT was used to investigate the ΔE_{ST} differences between Cy and Cy-NMNO [27]. The ΔE_{ST} value of Cy and Cy-NMNO were 0.87 eV and 1.06 eV, respectively (Fig. 3a and b). From the above investigations, Cy produced by releasing NO from Cy-NMNO exhibited smaller ΔE_{ST}, which is more conducive to promoting the ISC process and $^1O_2$ generation. The excellent $^1O_2$ yield improved the PDT performance.

Cytotoxicity assay and photoinduced cytotoxicity

The magnitude of cytotoxicity of nanoplatforms determines whether they can be applied in the clinic or not, therefore, we examined the cytotoxicity under non-laser irradiation using Cell Counting Kit-8 (CCK-8 kit). First, we divided the cells into three groups, control, Cy@SiO_2 group, and Cy-NMNO@SiO_2 group. The Control group was left untreated, and the Cy@SiO_2, Cy-NMNO@SiO_2 groups were added with 0, 2, 4, 6, 8, 10 μg/mL of Cy@SiO_2, Cy-NMNO@SiO_2, respectively. As shown in Fig. 4a, after incubation of A375 cells with Cy-NMNO@SiO_2 at a concentration of 10 μg/mL for 24 h, more than 85% of the cells survived. This proves that our synthesized nanoplatform Cy-NMNO@SiO_2 has low cytotoxicity and can be applied to cell viability. After confirming the good in vitro biosafety of Cy-NMNO@SiO_2, we proceeded to evaluate its tumor cell killing ability. As can be seen in Fig. 4b, the cell survival rate of the control group did not significantly decrease under 808 nm laser irradiation (1.5 W/cm^2, 5 min). The cytotoxicity of Cy@SiO_2, Cy-NMNO@SiO_2 showed a concentration-dependent pattern, and as the concentration of Cy@SiO_2, Cy-NMNO@SiO_2 (0–10 μg/mL) increased, the survival rate of the cells gradually decreased, and the cell survival rate was almost zero when the Cy-NMNO concentration was 10 μg/mL. And it can be seen from the figure that the phototoxicity of Cy-NMNO@SiO_2 was significantly higher than that of Cy@SiO_2 group. This confirms our speculation that under NIR laser irradiation, the chemical bond between Cy-NMNO is broken, producing both Cy and NO. Cy has a photodynamic therapeutic effect, and nitric oxide (NO) binds to the oxygen-binding site of mitochondria, inhibiting cellular respiration and reducing endogenous O_2 consumption, and also synergistically enhances the photodynamic therapy efficacy. NO can react with superoxide in the tumor environment to form oxidant peroxynitrite ($ONOO^-$) and synergistically enhance the anti-hypoxic photodynamic effect. NO can react with superoxide anions in the tumor environment to form the oxidant peroxynitrite ($ONOO^-$), which

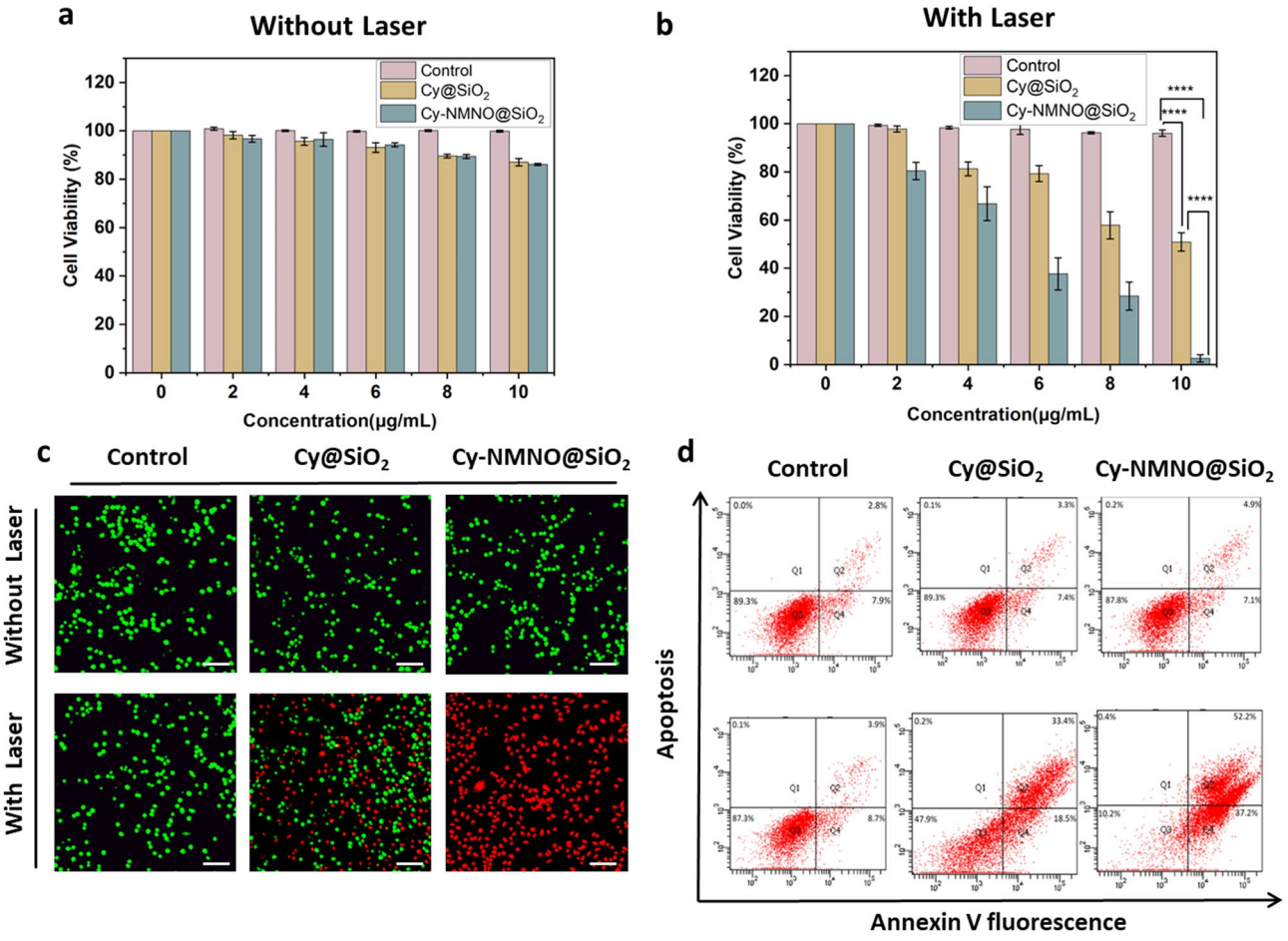

Fig. 4 (**a**) (**b**) The cytotoxicity of A375 cells treated with PBS, Cy@SiO_2, Cy-NMNO@SiO_2 under laser irradiation and without laser irradiation (****$P < 0.0001$). (**c**) Calcein AM/PI co-staining imaging of A375 cells treated with PBS, Cy@SiO_2, Cy-NMNO@SiO_2 under laser irradiation and without laser irradiation was observed using laser scanning confocal microscopy. Scale bar = 200 μm. (**d**) Apoptosis was analyzed using flow cytometry under laser irradiation and without laser irradiation in control, Cy@SiO_2, Cy-NMNO@SiO_2 (808 nm, 1.5 W/cm^2, and 5 min)

synergistically enhances the anti-hypoxic photodynamic effect.

Next, we continue to confirm our speculation by Calcein AM/PI Cell Activity and Cytotoxicity Assay Kit, Annexin V-FITC Apoptosis Kit, Western blot, etc. Calcein/PI Cell Activity and Cytotoxicity Assay Kit is a very convenient kit for the detection of dead and alive animal cells based on double fluorescence staining method of Calcein-AM (calcineurin) and PI (Propidium Iodide) dual fluorescence staining method to detect the dead and alive animal cells, which is based on the principle that the two probes detect the intracellular esterase activity and cell membrane integrity, respectively, and thus respond to the cell's live and dead status. Calcein AM stained live cells in green, while Propidium Iodide (PI) stained dead cells in red. As can be seen from the Fig. 4c, in the absence of laser irradiation, all A375 cells were green and not dead. While some cells in the Cy@SiO_2 group died under laser irradiation, almost all cells in the Cy-NMNO@SiO_2 group died. This is consistent with the results of our CCK-8 assay, which showed that the phototoxicity of Cy-NMNO@SiO_2 was significantly higher than that of Cy@SiO_2 group. In addition, we also verified the results with Annexin V-FITC apoptosis kit and statistically analyzed to obtain that the apoptosis rate of Cy-NMNO@SiO_2 was significantly higher than that of Cy@SiO_2 group (Fig. 4d, S5) ($P<0.0001$).

It is well known that the microenvironment of many solid tumors is hypoxic. In particular, the constant consumption of oxygen to generate cell-damaging ROS during PDT further exacerbates tumor hypoxia, severely impeding the generation of efficient ROS and leading to suboptimal PDT efficiency [28]. Hypoxia-inducible factor-1α (HIF-1α) is a nuclear transcription factor produced by cells in response to hypoxia and is a major member of the hypoxia-inducible factor family. It is normally located in the cytoplasm, and the α-subunit is rapidly ubiquitinated and degraded when the intracellular oxygen partial pressure is normal. However, under hypoxia, HIF-1α accumulates, translocates from the cytoplasm to the nucleus and binds to the β-subunit, initiating a series of genes that contribute to the adaptation of cells to hypoxia, and HIF-1α is the major hypoxia-associated gene [29–31]. To verify the hypoxia tolerance of Cy-NMNO@SiO_2, the expression of HIF-1α was detected by Western blot after Cy-NMNO@SiO_2 was applied to A375 cells with different irradiation times. As shown in Fig. 5a, b, c, d and e, the cell-related apoptotic proteins Bax, Caspase-9, Cytochrome C increased with irradiation time, which proved that our nanoplatform Cy-NMNO@SiO_2 did have a therapeutic effect on PDT. However, the expression of HIF-1α decreased with irradiation time. This suggests that our nanoplatform Cy-NMNO@SiO_2 can ultimately generate NO under NIR laser irradiation. NO, as an important vasotension-regulating messenger, can achieve the alleviation of tumor hypoxia [32].

To reconfirm our speculation, we injected different therapeutic drugs Cy@SiO_2, Cy-NMNO@SiO_2 intravenously into the homozygous BALB/c mice using PBS as a control, respectively. As shown in the Fig. 5f, g, h, i and j, the apoptotic protein expression of Cy-NMNO@SiO_2 group was significantly higher than that of the control group and the Cy@SiO_2 group ($P<0.05$), but the expression of HIF-1α was significantly lower than the control and Cy@SiO_2 groups ($P<0.05$). These results above suggest that Cy-NMNO@SiO_2 on the one hand can generate sufficient ROS to significantly amplify oxidative stress in vivo for tumor PDT therapy. However, in the case of PDT alone, the treatment exacerbates the hypoxic environment at the tumor site, whereas the precisely controlled release of NO at the tumor site helps to alleviate the hypoxia at the tumor site and synergistically enhances the effect of PDT treatment. The above experiments confirm that our nanoplatform can indeed achieve the treatment of skin cancer and improve the high hypoxia at the tumor site due to the consumption of oxygen by PDT.

Antimicrobial testing

Current clinical strategies to combat bacteria focus on antibiotic therapy. However, these strategies face increasing challenges due to the development of drug-resistant bacteria. The era of antibiotic drugs as the mainstay against harmful bacteria is reportedly over. Therefore, in order to protect public health, there is an urgent need for research and development of innovative antimicrobial agents with high antimicrobial activity and without inducing bacterial resistance. Photodynamic therapy (PDT)-based antimicrobial agents may be a promising alternative.

Next, we validated the antibacterial effect of the nanoplatform Cy-NMNO@SiO_2. The dilution plate method was used to evaluate the synergistic PDT/NO bactericidal effect of Cy-NMNO@SiO_2 against Gram-positive bacteria (Staphylococcus aureus). Staphylococcus aureus was inoculated in liquid medium of Luria-Bertani (LB) and incubated overnight at 37 °C in an incubator with shaking. Staphylococcus aureus was randomly divided into three groups, control group, Cy@SiO_2 group and Cy-NMNO@SiO_2 group, and according to their groupings, the same concentration of PBS, Cy@SiO_2, Cy-NMNO@SiO_2 were added and irradiated (808 nm, 1.5 W/cm^2, 5 min) with and without irradiation, respectively. As shown in Fig. 6a, the number of colonies in the Cy@SiO_2 + NIR-treated group was significantly reduced compared with the control, Cy@SiO_2 group and Cy-NMNO@SiO_2 without 808 nm laser irradiation. The inactivation rate reached 36.4% in the Cy@SiO_2 + NIR group (Fig. 6b).

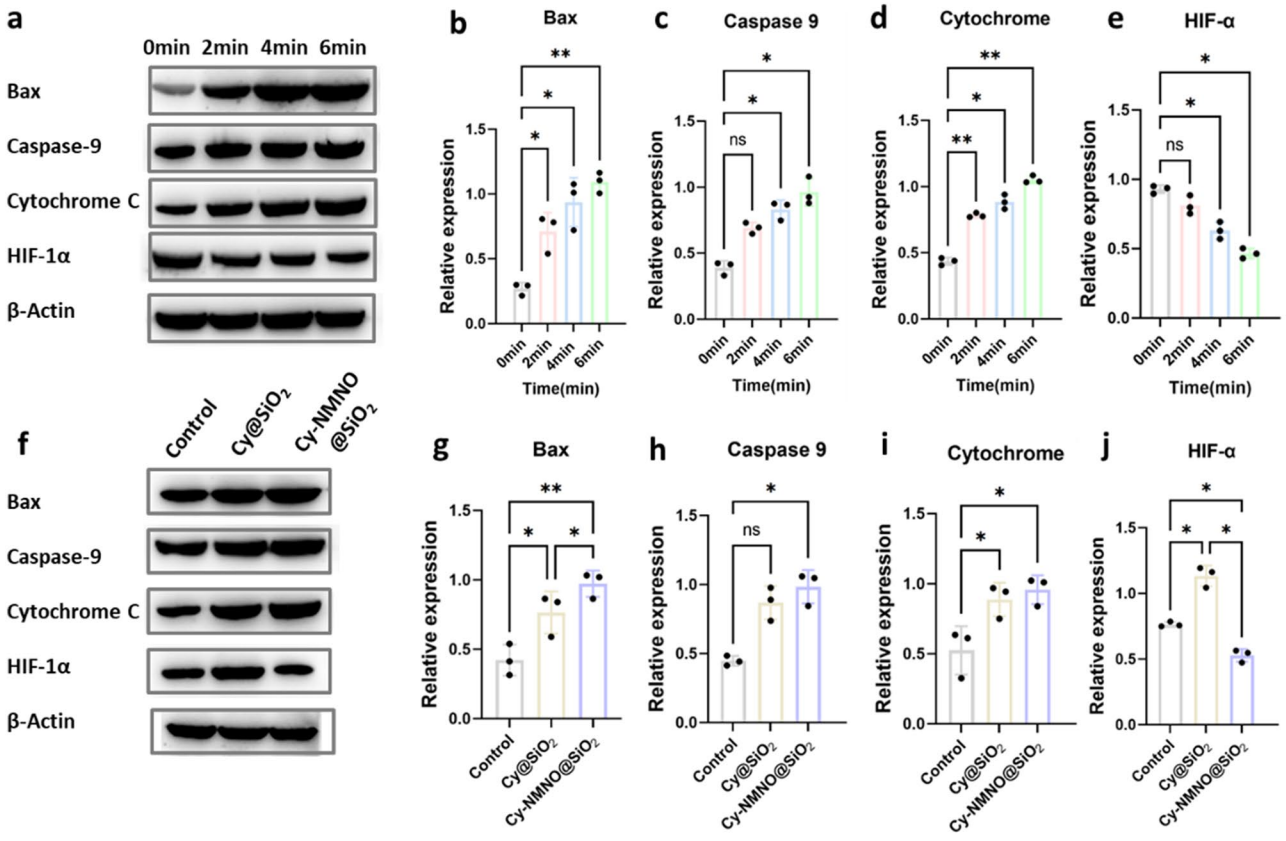

Fig. 5 (**a**) Protein expression of Bax, Caspase-9, Cytochrome C, HIF-1α of A375 cells treated with PBS, Cy@SiO_2, Cy-NMNO@SiO_2 were laser at different times using western blot analysis and using the expression of β-actin as a control. (**b**) (**c**) (**d**) (**e**) Quantitative analysis of Bax, Caspase-9, Cytochrome C, HIF-1α expression in (**a**). (**f**) Protein expression of Bax, Caspase-9, cytochrome C, and HIF-1α in A375 tumor-bearing mice with various treatments, and β-actin expression was used as a control. (**g**) (**h**) (**i**) (**j**) Quantitative analysis of Bax, Caspase-9, Cytochrome C, HIF-1α expression in (**f**)

Cy, as a photosensitizer, can produce reactive oxygen species, which has a therapeutic effect on photochemotherapy. In the Cy-NMNO@SiO_2 + NIR group, only a small amount of bacteria survived, and the inactivation rate was as high as 94.4%.

This indicates that NO was released from the photosensitizer during laser irradiation. NO is a typical lipophilic biosignaling molecule, a broad-spectrum antimicrobial candidate, and its antimicrobial process does not depend on the type of bacteria compared with traditional antibiotics. NO is able to produce additional $ONOO^-$, RNS, etc. in bacteria and the by-products of NO are able to disrupt bacterial cell membranes due to nitrosation and oxidative stress [33]. It also induces significant DNA damage, which makes the bacteria more susceptible to damage and thus has a bactericidal effect. Gram-negative bacteria have an additional membrane layer in their cell wall structure compared to Gram-positive bacteria, which makes it often difficult for typical PDT agents to penetrate these bacteria. However, our small molecule photosensitizer Cy has a positive charge and bacteria have a negative charge, which can enhance the interaction between the photosensitizer and the bacterial outer membrane and improve its PDT antimicrobial properties. Therefore, we similarly tested the antimicrobial effect of Cy-NMNO@SiO_2 against E. coli (Gram-negative bacteria). As shown in Fig. 6c, the bacterial growth was normal without NIR laser irradiation, but only a small amount of bacteria survived in the Cy-NMNO@SiO_2 + NIR group, with an inactivation rate of 96.6% (Fig. 6d). This proves that the Cy-NMNO@SiO_2 also has a good antibacterial effect on Gram-negative bacteria under NIR light irradiation.

In vivo imaging and anti-tumor therapy in tumor-bearing mice

In vivo bioimaging plays a crucial role in the accurate diagnosis and treatment of tumors. Since Cy-NMNO can have "off-on" fluorescence activation under near-infrared laser irradiation, we utilized this property to study the in vivo activation of Cy-NMNO@SiO_2 in mice. When the tumor volume of A375 ruffed mice increased to about 150 mm^3, Cy-NMNO@SiO_2 was injected through the tail vein. The fluorescence signal at the tumor site of ruffed mice was gradually

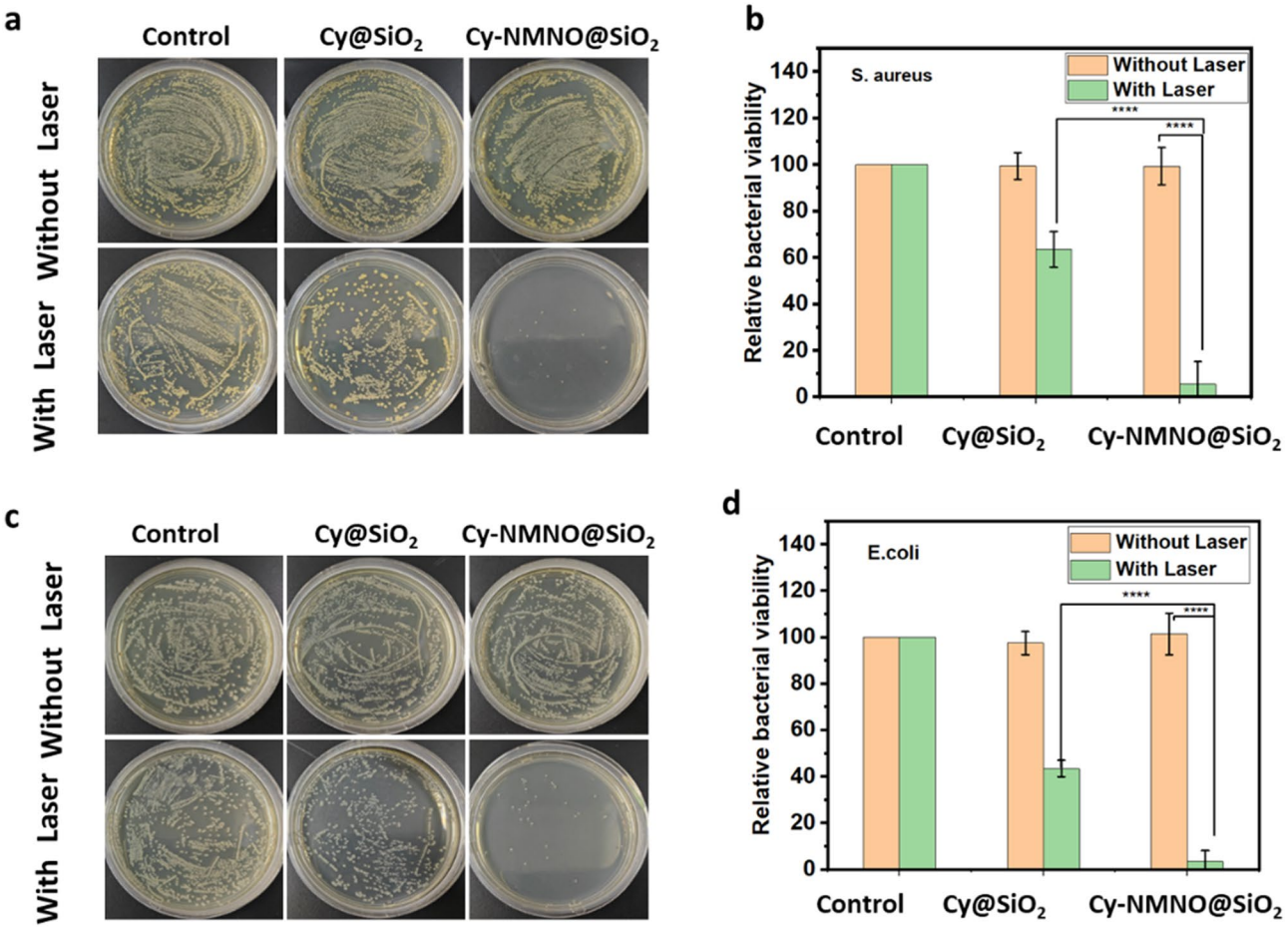

Fig. 6 Photographs of bacterial colonies formed by (**a**) S. aureus (**c**) E. coli based on plate count method. The corresponding bacterial viabilities of **b**) S. aureus **d**) E. coli. Treated with PBS, Cy-Cy@SiO_2, Cy-NMNO@SiO_2 without or with 808 nm laser irradiation (1.5 W cm^{-2}, 5 min) (****$P < 0.0001$)

enhanced after 808 nm laser irradiation. We euthanized the mice at 0 h, 6 h, 12 h, 24 h and 36 h, respectively, and quantitatively analyzed the fluorescence intensity of each group by ImageJ software after being photographed by a fluorescence imaging system. The schematic illustration of treatment route was shown in Fig. 7a. As shown in Fig. 7b, the fluorescence of the tumor tissue appeared 6 h after the intravenous injection of Cy-NMNO@SiO_2, reached the maximum intensity at 12 h, and then gradually weakened. These data indicate that Cy-NMNO@SiO_2 can be activated under near-infrared light irradiation to produce Cy and realize fluorescence imaging.

In order to study the therapeutic effect of Cy-NMNO@SiO_2 on the mouse skin melanoma model, when the volume tumor volume of A375 loaded mice reached about 150 mm^3, we randomly divided the loaded mice into 6 groups: PBS group, PBS + Laser group, Cy@SiO_2 group, Cy@SiO_2 + Laser, Cy-NMNO@SiO_2, and Cy- NMNO@SiO_2 + Laser groups, 10 mice in each group. We recorded the body weights and tumor volumes of the mice (at 2-day intervals after irradiation) and calculated the relative tumor volumes of the mice. (Fig. 7c, d, and f). The relative tumor volumes of the PBS + Laser group both increased by about 5.5-fold, indicating that single laser irradiation had little effect on tumor growth.

Although the Cy@SiO_2 + Laser group had a certain inhibitory effect on the tumor treatment, the tumor volume was still increasing gradually, and it failed to achieve the effect of completely treating the tumor. Notably, the Cy-NMNO@SiO_2 + NIR group showed significant tumor inhibition with no regrowth. Meanwhile, combined with the results of Western blot above, Cy-NMNO was shown to be an effective synergistic PDT-GT tumor therapeutic agent. In order to further observe the killing ability of Cy-NMNO@SiO_2 on tumor tissues after treatment to verify its antitumor effect. We observed the status of tumor tissues by hematoxylin & eosin (H&E) staining (Fig. 7e). H&E staining showed that the tumor tissue damage in Cy-NMNO@SiO_2 + Laser group was obvious, and the efficacy was significant. While PBS, PBS + Laser, Cy@SiO_2 group, and Cy-NMNO@SiO_2 did not show significant

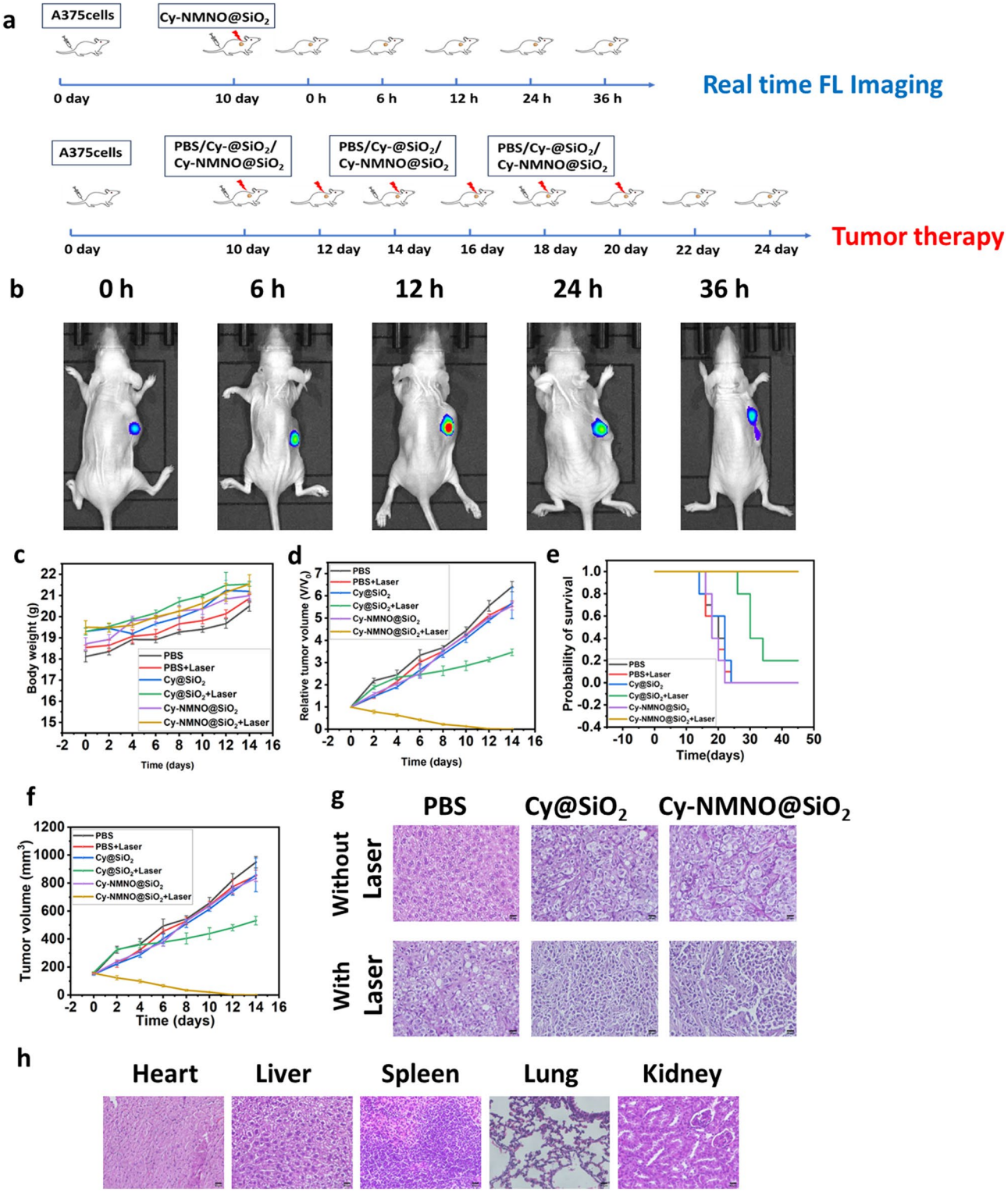

Fig. 7 (**a**) Schematic illustration of treatment route. (**b**) Real-time fluorescence imaging in A375 tumor-bearing mice (**c**) Body weight change, (**d**) Relative tumor volume, (**e**) Probability of survival, (**f**) Tumor volume of A375 tumor-bearing mice with various treatments. (**g**) H&E staining of tumor after various treatments. Scale bar = 20 μm. (**h**) Results of H&E staining of heart, liver, spleen, lung and kidney of surviving mice in the Cy-NMNO@SiO_2 + laser treatment group. Scale bar = 20 μm

tumor damage. The Cy@SiO_2 group + Laser group had some therapeutic effect on the tumor, but the therapeutic effect was limited. Meanwhile, in order to explore the in vivo safety during antitumor treatment, the weight of the hormonal mice was recorded during the tumor suppression experiments in hormonal mice, and the mice were weighed every other day. And the survival rate of mice was calculated (Fig. 7e). As shown in Fig. 7c, there was no significant change in the body weight of all mice, and the mice in the Cy-NMNO@SiO_2 + Laser treatment group always survived. In order to prove the safety of the nanoplatform again, we observed the normal organs (heart, liver, spleen, lung and kidney) of the surviving mice in Cy-NMNO@SiO_2 by sectioning and found that there was no obvious damage to the heart, liver, spleen, lungs, kidneys and other organs of the mice. This indicates that Cy-NMNO@SiO_2 has good biosafety in the therapeutic dose range with negligible side effects. It can be seen that Cy-NMNO@SiO_2 can effectively treat tumors under near-infrared laser irradiation without obvious toxic side effects.

Conclusion

In summary, we designed and synthesized a multifunctional nanoplatform Cy-NMNO@SiO_2, which is a probe Cy-NMNO loaded into mesoporous silica to achieve drug delivery. Cy-NMNO is capable of releasing small molecules of photosensitizer and NO at the same time by coupling NO donor to photosensitizer Cy, which is capable of releasing small molecules of photosensitizer and NO simultaneously by breaking the N-N bond between the probes under the NIR laser irradiation, to achieve the synergistic treatment of anti-tumor antibacterial PDT-GT. In this system, Cy can be used as a photosensitizer to generate $^1O_2$ under 808 nm irradiation to achieve PDT therapeutic effect, and NO can inhibit cellular respiration, reduce endogenous O_2 consumption, widen the tumor blood vessels, and improve the hypoxia of the tumor site. At the same time, NO can generate toxic $ONOO^-$ with superoxide anion in the cells to directly kill tumor cells, thus achieving more effective tumor treatment than conventional PDT. Meanwhile, Cy-NMNO@SiO_2 also showed significant bactericidal effects against Gram-negative and Gram-positive bacteria. In summary, Cy-NMNO@SiO_2 has good antimicrobial and antitumor therapeutic effects, and the NO produced can alleviate the hypoxia caused by PDT and improve the therapeutic efficacy of PDT, and this work may provide a promising approach for synergistic PDT-GT.

Supplementary Information

The online version contains supplementary material available at https://doi.org/10.1186/s12951-024-02878-7.

Supplementary Material 1

Acknowledgements
Not applicable.

Author contributions
L. F.: Conceptualization, Validation, Formal analysis, Investigation, Writing - original draft, Y. H.: Conceptualization, Software, Visualization, Writing - review & editing, X. S.: Data curation, Methodology, Investigation, X. S.: Data curation, Methodology, Investigation, X. W.: Data curation, Methodology, Investigation, X. W.: Conceptualization, Funding acquisition, Methodology, Writing - review & editing, L. C.: Funding acquisition, Methodology, Writing - review & editing, S. Y.: Funding acquisition, Conceptualization, Methodology, Writing - review & editing.

Funding
This work was supported by the National Natural Science Foundation of China (Nos. 21804010, 22376216, 21976209, 22007005), the Research Initiation Fund of Binzhou Medical University (Grant No. BY2019KYQD39, BY2020KYQD01 and 50012304601), Taishan Scholar Project Special Funding (No. ts20190962), Shandong Peninsula Engineering Research Center of Comprehensive Brine Utilization (2018LS014).

Data availability
No datasets were generated or analysed during the current study.

Declarations

Ethics approval and consent to participate
All animal procedures were performed in accordance with the Guidelines for Care and Use of Laboratory Animals of Binzhou Medical University and approved by the Institutional Animal Care and Use Committee of Binzhou Medical University (Yantai, China) (Approval Number: 2023 – 125).

Consent for publication
Not applicable.

Competing interests
The authors declare no competing interests.

Author details
[1]School of Pharmacy, Binzhou Medical University, Yantai 264003, China
[2]CAS Key Laboratory of Coastal Environmental Processes and Ecological Remediation, Yantai Institute of Coastal Zone Research, Chinese Academy of Sciences, Yantai 264003, China
[3]College of Chemistry, Chemical Engineering and Materials Science, Shandong Normal University, Jinan, Shandong 250014, China
[4]Department of Intelligent Manufacturing, Shandong City Service Institute, Yantai 264003, China

Received: 12 June 2024 / Accepted: 26 September 2024
Published online: 01 October 2024

References

1. Sun J, Cai X, Wang C, Du K, Chen W, Feng F, Wang S. Cascade reactions by Nitric Oxide and Hydrogen Radical for Anti-hypoxia Photodynamic Therapy using an Activatable Photosensitizer. J Am Chem Soc. 2021;143:868–78.
2. Zhang C, Xia DL, Liu JH, Huo D, Jiang XQ, Hu Y. Bypassing the immunosuppression of myeloid-derived suppressor cells by reversing Tumor Hypoxia using a platelet-inspired platform. Adv Funct Mater. 2020;30:2000189–200207.

3. Zhang C, Yuan YF, Wu KJ, Wang Y, Zhu ST, Shi JY, Wang LH, Li Q, Zuo XL, Fan CH, Chang C, Li J. Driving DNA Origami Assembly with a Terahertz Wave. Nano Lett. 2022;22:468–75.
4. Li L, He SH, Liao BY, Wang MC, Lin HM, Hu B, Lan XY, Shu ZL, Zhang C, Yu M, Zou ZW. Orally Administrated Hydrogel Harnessing Intratumoral Microbiome and Microbiota-Related Immune responses for Potentiated Colorectal Cancer Treatment. Research-China. 2024;7:1–21.
5. Huang H, Zhang C, Wang XL, Shao JS, Chen C, Li HM, Ju CM, He J, Gu HY, Xia DL. Overcoming hypoxia-restrained Radiotherapy using an erythrocyte-inspired and glucose-activatable platform. Nano Lett. 2020;20:4211–9.
6. Zuo HQ, Tao JX, Shi H, He J, Zhou ZY, Zhang C. Platelet-mimicking nanoparticles co-loaded with WO and metformin alleviate tumor hypoxia for enhanced photodynamic therapy and photothermal therapy. Acta Biomater. 2018;80:296–307.
7. Xu J, Zeng F, Wu H, Hu C, Yu C, Wu S. Preparation of a mitochondria-targeted and NO-releasing nanoplatform and its enhanced pro-apoptotic effect on cancer cells. Small. 2014;10:3750–60.
8. Hu C, Cun X, Ruan S, Liu R, Xiao W, Yang X, Yang Y, Yang C, Gao H. Enzyme-triggered size shrink and laser-enhanced NO release nanoparticles for deep tumor penetration and combination therapy. Biomaterials. 2018;168:64–75.
9. An J, Hu YG, Li C, Hou XL, Cheng K, Zhang B, Zhang RY, Li DY, Liu SJ, Liu B, Zhu D, Zhao YD. A pH/Ultrasound dual-response biomimetic nanoplatform for nitric oxide gas-sonodynamic combined therapy and repeated ultrasound for relieving hypoxia. Biomaterials. 2020;230:119636.
10. Deng Y, Jia F, Chen S, Shen Z, Jin Q, Fu G, Ji J. Nitric oxide as an all-rounder for enhanced photodynamic therapy: Hypoxia relief, glutathione depletion and reactive nitrogen species generation. Biomaterials. 2018;187:55–65.
11. Khan FH, Dervan E, Bhattacharyya DD, McAuliffe JD, Miranda KM, Glynn SA. The role of nitric oxide in Cancer: Master Regulator or NOt? Int. J Mol Sci. 2020;21:9393.
12. Nwahara N, Motaung M, Abrahams G, Mashazi P, Mack J, Prinsloo E, et al. Dual singlet oxygen and nitric oxide-releasing silicon phthalocyanine for augmented photodynamic therapy. Mater Today Chem. 2022;26:101201.
13. Gayton J, Autry SA, Meador W, Parkin SR, Hill GJ, Hammer NI, Delcamp JH. Indolizine-cyanine dyes: Near Infrared Emissive Cyanine dyes with increased Stokes shifts. J Org Chem. 2019;84:687–97.
14. Zhu S, Tian R, Antaris AL, Chen X, Dai H. Near-Infrared-II Molecular dyes for Cancer imaging and surgery. Adv Mater. 2019;31:e1900321.
15. Huang Y, Liu Q, Wang Y, He N, Zhao R, Choo J, Chen L. Gold nanorods functionalized by a glutathione response near-infrared fluorescent probe as a promising nanoplatform for fluorescence imaging guided precision therapy. Nanoscale. 2019;11:12220–9.
16. Thananukul K, Kaewsaneha C, Opaprakasit P, Lebaz N, Errachid A, Elaissari A. Smart gating porous particles as new carriers for drug delivery. Adv Drug Deliv Rev. 2021;174:425–46.
17. Wen J, Yan H, Xia PY, Xu YQ, Li HJ, Sun SG. Mesoporous silica nanoparticles-assisted ruthenium(II) complexes for live cell staining. Sci China Chem. 2017;60:799–805.
18. Zhao T, Nguyen NT, Xie Y, Sun X, Li Q, Li X. Inorganic nanocrystals functionalized mesoporous silica nanoparticles: fabrication and enhanced bio-applications. Front Chem. 2017;5:118.
19. Rawat N, Sandhya K, Subaharan M, Eswaramoorthy G, Kaul. Comparative in vivo toxicity assessment places multiwalled carbon nanotubes at a higher level than mesoporous silica nanoparticles. Toxicol Ind Health. 2017;33:182–92.
20. Lu J, Liong M, Li Z, Zink JI, Tamanoi F. Biocompatibility, biodistribution, and drug-delivery efficiency of mesoporous silica nanoparticles for cancer therapy in animals. Small. 2010;6:1794–805.
21. Karimi M, Ghasemi A, Sahandi ZP, Rahighi R, Moosavi BS, Mirshekari H, Amiri M, Shafaei PZ, Aslani A, Bozorgomid M, Ghosh D, Beyzavi A, Vaseghi A, Aref AR, Haghani L, Bahrami S, Hamblin MR. Smart micro/nanoparticles in stimulus-responsive drug/gene delivery systems. Chem Soc Rev. 2016;45:1457–501.
22. Chang MY, Wang M, Liu YH, Liu M, Al Kheraif AA, Ma PA, Zhao YL, Lin J. Dendritic plasmonic CuPt alloys for closed-Loop Multimode Cancer Therapy with remarkably enhanced efficacy. Small 19 (2023).
23. Baeza A, Colilla M, Vallet-Regi M. Advances in mesoporous silica nanoparticles for targeted stimuli-responsive drug delivery. Expert Opin Drug Deliv. 2015;12:319–37.
24. Xing C, Deng J, Fu W, Li J, Xu L, Sun R, Wang D, Li C, Liang K, Gao M, Kong B. Interfacially Super-assembled Benzimidazole Derivative-based mesoporous silica nanoprobe for sensitive copper (II) detection and Biosensing in living cells. Chemistry. 2022;28:e202103642.
25. Wan MM, Chen H, Da WZ, Liu ZY, Yu YQ, Li L, Miao ZY, Wang XW, Wang Q, Mao C, Shen J, Wei J. Nitric oxide-driven Nanomotor for Deep tissue penetration and Multidrug Resistance reversal in Cancer Therapy. Adv Sci (Weinh). 2021;8:2002525.
26. Zhao J, Wu W, Sun J, Guo S. Triplet photosensitizers: from molecular design to applications. Chem Soc Rev. 2013;42:5323–51.
27. Wu WT, Zhang QG, Wang RQ, Zhao YF, Li ZT, Ning H, Zhao QS, Wiederrecht GP, Qiu JS, Wu MB. Synergies between Unsaturated Zn/Cu Doping sites in Carbon dots provide New pathways for Photocatalytic Oxidation. Acs Catal. 2018;8:747–53.
28. Yu M, Duan X, Cai Y, Zhang F, Jiang S, Han S, Shen J, Shuai X. Multifunctional Nanoregulator reshapes Immune Microenvironment and enhances Immune Memory for Tumor Immunotherapy. Adv Sci (Weinh). 2019;6:1900037.
29. Ke Q, Costa M. Hypoxia-inducible factor-1 (HIF-1). Mol Pharmacol. 2006;70:1469–80.
30. Semenza GL. Targeting HIF-1 for cancer therapy. Nat Rev Cancer. 2003;3:721–32.
31. Semenza GL. HIF-1 mediates metabolic responses to intratumoral hypoxia and oncogenic mutations. J Clin Invest. 2013;123:3664–71.
32. Vogel R. Listening to the endothelium: a story of signal and noise. J Am Coll Cardiol. 2008;51:1965–6.
33. Hetrick EM, Shin JH, Stasko NA, Johnson CB, Wespe DA, Holmuhamedov E, Schoenfisch MH. Bactericidal efficacy of nitric oxide-releasing silica nanoparticles. ACS Nano. 2008;2:235–46.

Publisher's note